PHOTONICS Research

All-fiber passively mode-locked laser using nonlinear multimode interference of step-index multimode fiber

Tao Chen,[1,*] Qiaoli Zhang,[1] Yaping Zhang,[1] Xin Li,[1] Haikun Zhang,[1] and Wei Xia[1,2]

[1]School of Physics and Technology, University of Jinan, Jinan 250022, China
[2]e-mail: sps_xiaw@ujn.edu.cn
*Corresponding author: taochen426@hust.edu.cn

Received 31 July 2018; revised 2 September 2018; accepted 11 September 2018; posted 13 September 2018 (Doc. ID 340879); published 16 October 2018

We experimentally demonstrate for the first time, to the best of our knowledge, an all-fiber passively mode-locked laser operation based on the nonlinear multimode interference of step-index multimode fiber. Such a structure couples the light in and out of the multimode fiber via single-mode fibers, and its physical mechanisms for saturable absorption have been analyzed theoretically based on the third-order nonlinear Kerr effect of multimode fiber. Using the nonlinear multimode interference structure with 48.8 mm length step-index multimode fiber, the modulation depth has been measured to be ~5%. The passively mode-locked laser output pulses have a central wavelength of 1596.66 nm, bandwidth of 2.18 nm, pulsewidth of ~625 fs, and fundamental repetition rate of 8.726 MHz. Furthermore, the influence of total cavity dispersion on the optical spectrum, pulse width, and output power is investigated systematically by adding different lengths of single-mode fiber and dispersion compensation fiber in the laser cavity.

https://doi.org/10.1364/PRJ.6.001033

1. INTRODUCTION

Passively mode-locked fiber lasers exhibit the advantages of compact and simple all-fiber structure, low-cost, and good compatibility with optical fiber systems. Various saturable absorption materials have been developed to actuate mode-locking based on a semiconductor saturable absorption mirror [1], single-walled carbon nanotube [2–4], and the 2D nanomaterials such as graphene [5–8], transition metal chalcogenides [9–11], topological insulators [12,13], and black phosphorus [14,15]. These materials often suffer from optical-power-induced thermal damage and oxidation, thus restricting the damage threshold and long-term stability of the fiber laser [16,17]. The alternative techniques to address the issues are the use of nonlinear polarization evolution [18,19], nonlinear amplifying loop mirror [20,21], and nonlinear mode-coupling [22]. Different from the precise control of the polarization state in nonlinear polarization evolution and the accurate selection of the coupler split ratio in a nonlinear amplifying loop mirror, the nonlinear mode-coupling can simply achieve stable and robust passive mode-locking through four structures. The first structure implementing nonlinear mode-coupling is the waveguide array coupling [22,23]. An AlGaAs waveguide array was used as a saturable absorber to experimentally achieve passive mode-locking in an Er-doped fiber laser (EDFL). Using the multicore fiber coupling is the second structure to mode-lock a fiber laser based on nonlinear mode-coupling [24–27]. The dual-core fiber couplers for a passively mode-locked fiber laser were numerically simulated, and a tapered seven-core telecommunication fiber for saturable absorption was experimentally measured. The third nonlinear mode-coupling structure is the long-period fiber grating coupling [28]. Although the long-period fiber grating is theoretically capable of supporting mode-locked fiber laser operation, the length required to achieve complete coupling is on the order of meters and limits its usefulness for mode-locked experiments. Nonlinear multimode interference (MMI) is the fourth structure to realize nonlinear mode-coupling [29–37]. The MMI structures usually consist of a multimode fiber (MMF) used as an intermediate coupler between two other fibers [e.g., single-mode fiber (SMF) or photonic crystal fiber]. They have been adopted for all-fiber bandpass filters with tens of centimeters of MMF and are also widely applied in the mode-field transformation between different types of fiber.

MMF is the key component of an MMI structure. Recently, graded-index multimode fibers (GIMFs) have attracted extensive investigation of nonlinear optical interactions [38,39], as the group velocities of all modes of the GIMF are nearly

identical at special wavelengths. Based on the GIMF in MMI structures, the mode-field adapters have been studied between the SMF and the photonic crystal fibers (NKT Photonics: LMA12, LMA15, and LMA20) [40,41]. Moreover, employing the nonlinear mode-coupling of SMF-GIMF-SMF structures, the stable mode-locked fiber lasers have been demonstrated in the all-normal-dispersion Tm-doped fiber laser [42], net-anomalous-dispersion EDFL [43–45], and all-normal-dispersion Yb-doped fiber laser [46]. For achieving mode-locking, the lengths of MMF should be precisely controlled on the order of the self-imaging distance. Self-imaging is the reproduction of the input field after coupling into the MMF and then propagating certain periodic lengths, and the length with one period is the self-imaging distance. The self-imaging distance of 50/125 GIMF is 1.15 mm [29]; it is too short to precisely process with a fiber cleaver, so the SMF-GIMF-SMF structures must be bent or stretched for adjusting the lengths of GIMF. Compared with GIMF, the self-imaging distances of 50/125 and 105/125 step-index multimode fibers (SIMFs) are 10.3 and 42.877 mm, respectively [47,48], and the lengths of SIMF are conveniently controlled under the self-imaging distance with the precision of a fiber cleaver. The passive Q-switching fiber laser has been reported by the use of MMI with 50/125 SIMF [49]. However, the features of the mode-locked fiber laser with the SIMF-based MMI are still unknown. In order to investigate the mode-locked features, here we employ the nonlinear MMI with 50/125 SIMF.

In this paper, the theory of nonlinear MMI with MMF is analyzed to realize saturable absorption. The theoretical lengths of SIMF for mode-locking are experimentally verified. The MMI is fabricated through splicing the SMF–SIMF–SMF structure with a fiber fusion splicer. Choosing 48.8 mm long SIMF, we present the passively mode-locked EDFL pulses of ~625 fs with a central wavelength of 1596.66 nm. Then, the influence of net cavity dispersion on the optical spectrum, pulse width, and output power is also investigated. Such an SMF–SIMF–SMF structure is promising for a simple and robust all-fiber mode-locked ultrafast laser.

2. NONLINEAR MULTIMODE INTERFERENCE

The MMI structure, as shown in Fig. 1, consists of an MMF between two SMFs, where L is the length of MMF. The SMFs are spliced onto the MMF to ensure that the mode field is launched in and out of the MMF segment. Ignoring the reflected loss, the propagating light field inside the SMF is coupled into many guided modes of the MMF at the splicing point ($z = 0$) between the input SMF and the MMF, as follows [29]:

$$E_{\mathrm{SMF}}(r,\phi,z=0)=\sum_{n=1}^{N} C_n e_n(r,\phi,z=0), \tag{1}$$

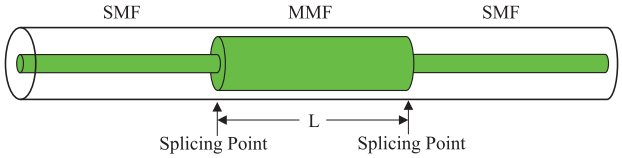

Fig. 1. Diagram of MMI structure.

where $E_{\mathrm{SMF}}(r,\phi,z=0)$ is the fundamental mode of the SMF, $e_n(r,\phi,z=0)$ is the nth guided mode of the MMF, N is the number of excited modes inside the MMF, and C_n is the mode expansion coefficient.

After coupling, the light field propagates along the MMF with all excited modes and can be expressed as

$$\begin{aligned} E_{\mathrm{MMF}}(r,\phi,z) &= \sum_{n=1}^{N} C_n e_n(r,\phi,0) e^{-i\beta_n z} \\ &= e^{-i\beta_1 z}\sum_{n=1}^{N} C_n e_n(r,\phi,0) e^{-i(\beta_n-\beta_1)z}, \end{aligned} \tag{2}$$

where β_1 and β_n are the propagation constants of the fundamental mode and the nth guided mode of the MMF, respectively. At some periodic positions inside the MMF, the reproduction of the input field (self-imaging) occurs. The all-excited modes of the MMF are in phase and satisfy the following condition:

$$\beta_1 L_S + q2\pi = \beta_n L_S, \tag{3}$$

where q is an integer, and L_S is the self-imaging distance with one period. L_S can be calculated through the fully vectorial mode expansion approach [50], and $L_S = 10.3$ mm for 50/125 SIMF [47].

In the intracavity of the fiber laser, the optical power is high enough to consider the self-phase modulation (SPM) and the cross-phase modulation (XPM) effects. We ignore the loss, the walk-off, and the four-wave mixing (FWM) effects in the MMF due to its short length. Similar to the derivation of third-order nonlinear couple-mode equations in a photonic crystal waveguide [51], the coupled-mode equations for the propagation of all excited modes can be expressed as

$$\frac{\partial A_n}{\partial z}=\frac{i n_2\omega_0}{c}\left(f_{nn}|A_n|^2+2\sum_{m\neq n} f_{mn}|A_m|^2\right)A_n, \tag{4}$$

where A_n and A_m are the normalized complex amplitudes of the nth and mth guided mode, respectively. n_2 is the nonlinear Kerr coefficient, and ω_0 is the angular frequencies of all modes. f_{nn} and f_{mn} are the overlap of fields for SPM and XPM, respectively. f_{mn} is calculated by

$$f_{mn}=\frac{\iint |e_m(x,y)|^2|e_n(x,y)|^2\mathrm{d}x\mathrm{d}y}{\iint |e_m(x,y)|^2\mathrm{d}x\mathrm{d}y \iint |e_n(x,y)|^2\mathrm{d}x\mathrm{d}y}, \tag{5}$$

where $e_m(x,y)$ and $e_n(x,y)$ are the field distributions. The well-known effective interaction area is defined by $A_{mn}^{\mathrm{eff}}=\frac{1}{f_{mn}}$. We consider $\gamma_n=\frac{n_2\omega_0 f_{nn}}{c}$ and $P_n=|A_n|^2+2\sum_{m\neq n}\frac{f_{mn}}{f_{nn}}|A_m|^2$; then Eq. (4) can be expressed as

$$\frac{\partial A_n}{\partial z}=i\gamma_n P_n A_n, \tag{6}$$

where γ_n is the nonlinear coefficient, and P_n is the equivalent optical power for the nth mode. γ_1 and P_1 for the fundamental mode are the maximum values, respectively. From Eq. (6), we can obtain

$$A_n(z)=A_n(0)e^{i\gamma_n P_n z}, \tag{7}$$

where $A_n(0)$ is the initial amplitude of the nth mode. Thus, the SPM and XPM bring about an additional phase shift $\gamma_n P_n z$ in

the MMF [52]. Equation (3) for the self-imaging condition can be rewritten as follows:

$$\beta_1 L_S' + q2\pi + \gamma_1 P_1 L_S' = \beta_n L_S' + \gamma_n P_n L_S', \tag{8}$$

where L_S' is the amendatory self-imaging distance. Combining Eqs. (3) and (8), we can have

$$L_S' = \frac{\beta_1 - \beta_n}{(\beta_1 - \beta_n) + (\gamma_1 P_1 - \gamma_n P_n)} L_S. \tag{9}$$

Based on Eq. (9), there are two mechanisms for realizing MMI mode-locking with different lengths of MMF. One is with L slightly smaller than nL_S, where n is an integer. For a high power signal, $L \approx nL_S'$ and MMI experience the higher transmission than for a low power signal. The other is with L around $(n + 1/2)L_S$. For a low power signal, MMI sustains the lower transmission than for the high power signal.

In order to prove the mechanisms in the experiments of a passively mode-locked fiber laser, we fabricate the MMI structures for degressive L from 75 mm ($\sim 7L_S$) to 32 mm ($\sim 3L_S$) with 1 mm step size. The L is short enough to avoid the bandpass filtering of MMI and can be easily controlled by using a fiber fusion splicer (Fujikura FSM-60S) and a fiber cleaver (SUMITOMO FC-6S) together with a Vernier caliper.

3. EXPERIMENTAL SETUP

The experimental setup of the passively mode-locked EDFL with a ring cavity configuration is presented in Fig. 2. A 1.5 m high concentration EDF (OFS EDF-80) is used as the gain medium and is pumped by a 980 nm high power laser diode (Connet Venus-980) via a 980/1550 nm wavelength division multiplexer (WDM) coupler. An intracavity polarization controller (PC) is used to adjust the linear cavity birefringence, while a polarization-independent isolator maintains the unidirectional laser pulse propagation. The SMF or DCF is added in the cavity to change the total cavity dispersions. The MMI is inserted into the cavity between the PC and the coupler. The polarization-dependent losses of couplers, WDM, and optical isolator are less than 0.1 dB. The generated mode-locked pulses are directed out by use of a 90:10 coupler and then pass through another 90:10 coupler. The pulses are simultaneously monitored by an optical spectrum analyzer (OSA, YOKOGAWA AQ6370B) with 0.02 nm resolution and a high-speed photodetector (New Focus 1611, 1 GHz) connected to an oscilloscope (Tektronix MDO 3102, Mixed Domain Oscilloscope).

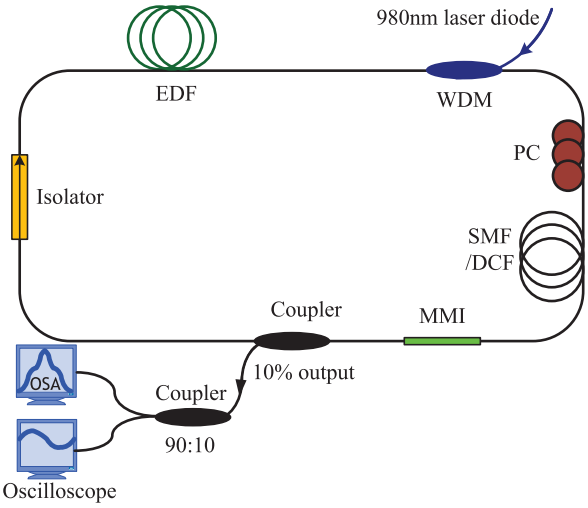

Fig. 2. Experimental setup of the nonlinear MMI mode-locked fiber laser. WDM, wavelength division multiplexer; PC, polarization controller; DCF, dispersion compensation fiber; OSA, optical spectrum analyzer.

The group velocity dispersion (GVD) plays an important role in maintaining stability of the mode-locked fiber laser. The GVD of the EDF used in the system is –46.25 ps/(nm·km) and that of the SMF is 18 ps/(nm·km), at the wavelength of 1560 nm. For our fiber laser, the central wavelength is around 1597 nm, and the negligible difference of GVD can be ignored. The initial length of the laser cavity is ~11.1 m; thus, the round-trip dispersion of the whole cavity is ~ -0.139 ps^2.

4. RESULTS AND DISCUSSION

A. Optical Property of MMI

It is well known that the soliton pulses are the result of a balance between cavity dispersion and third-order nonlinear effects (SPM, XPM, and FWM). The mode-locked fiber lasers are easy to adjust for large net anomalous GVD. We add 10 m SMF in the confirmatory experiments for MMI mode-locked mechanisms, and the total dispersion is ~ -0.383 ps^2. To experimentally prove the mechanisms, the MMI structures with different lengths of SIMF are connected in the cavity. It is found that the mode-locked operation can be realized under many different lengths, and the selective optical spectra are shown in Fig. 3. $L = 59$ mm and 49 mm are slightly smaller than $6L_S$ and $5L_S$ when $L = 55$ mm and 43 mm are, respectively, around $(5 + 1/2)L_S$ and $(4 + 1/2)L_S$. The laser operates in Q-switched mode-locking state for the $L = 59$ mm case, while the left peak is not completely suppressed, and there is a continuous wave (CW) component in the optical spectrum for the $L = 55$ mm case. For the $L = 49$ mm and $L = 43$ mm cases, the optical spectra show the typical feature of solitons and also contain CW components. These optical spectra can be optimized by further controlling the lengths of SIMF.

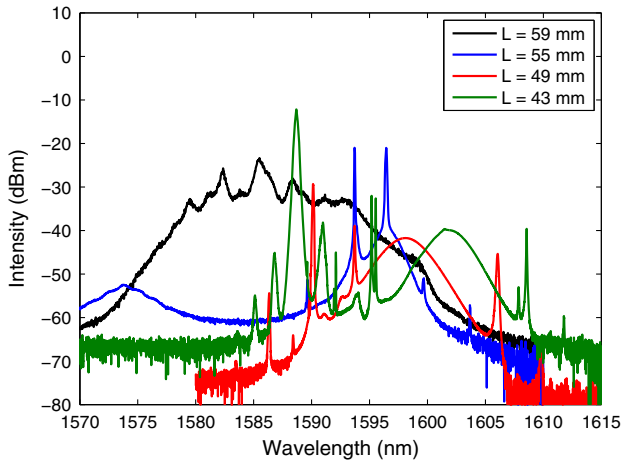

Fig. 3. Optical spectra of mode-locked fiber lasers with different lengths of MMF in MMI structures.

In the following, we choose the MMI with $L \approx 49$ mm for the all-fiber passively mode-locked laser. After some optimization experiments eliminating the CW component of the optical spectrum and reducing the mode-locking threshold, the final length of the SIMF is $L = 48.8$ mm. The optical property of saturable absorption of the 48.8 mm long MMI is measured by a homemade fs fiber laser with another MMI, as shown in Fig. 4(a). The fs fiber laser (central wavelength of 1598.8 nm, pulse width of ~834 fs, and repetition rate of 11.18 MHz) is amplified by a homemade Er-doped fiber amplifier. After passing through a PC, the fs pulses are injected into the MMI via an attenuator and a coupler, and then the powers are measured by a power meter (Thorlabs 100D, S155C). Within the output power range of the pulsed fiber laser, the absorption of the MMI is measured, and the obtained results are shown in Fig. 4(b). The experimental errors come from the connecting the fiber pigtail with the power meter. At a low input power level, the transmission of MMI is around ~57.0% and the corresponding linear loss is around ~43.0%. When the average input power of the pulses is raised to 6 mW, the transmission increased by ~5% due to the absorption saturation. The modulation depth is comparable with those of the 2D materials, and the linear loss and the saturable power are relatively lower [5–15]; thus, the mode-locking threshold based on the gain of the EDF can be very low. These indicate that the MMI can be used to generate stable and low-noise laser pulses in the fiber lasers.

B. MMI-Based Mode-Locked Fiber Laser

The pump threshold of the CW operation laser is ~26 mW. Increasing the pump power to 56 mW and slightly tuning the PC, the fiber laser can operate in the steadily mode-locked state. The stability of the mode-locked fiber laser is important [16,17] and can be enhanced through cooling the saturable absorber [53]. Being superior to the saturable absorption materials, the SiO_2 of the MMI can support the high threshold of optical-power-induced thermal damage at room temperature and lead to long-term reliability of a mode-locked fiber laser. We test our system over 24 h, and the mode-locked operation guarantees a stable optical spectrum, pulse width, output power, and repetition rate. During the operation, the pump power may be increased to 97 mW with little change of the pulse width. Under 90 mW pump power, the optical spectrum is shown in Fig. 5(a). The full width at half-maximum (FWHM) bandwidth is 2.18 nm, and the central wavelength is 1596.66 nm. As shown in Fig. 5(a), the wavelength range of mode-locked operation with MMI is consistent with the CW operation without MMI. The Kelly sidebands, resulting from the intracavity periodical perturbation, clearly appear with discrete and well-defined peaks in the optical spectrum. The mth order of Kelly sideband position relative to the central wavelength for a chirp-free soliton can be obtained from [54,55]

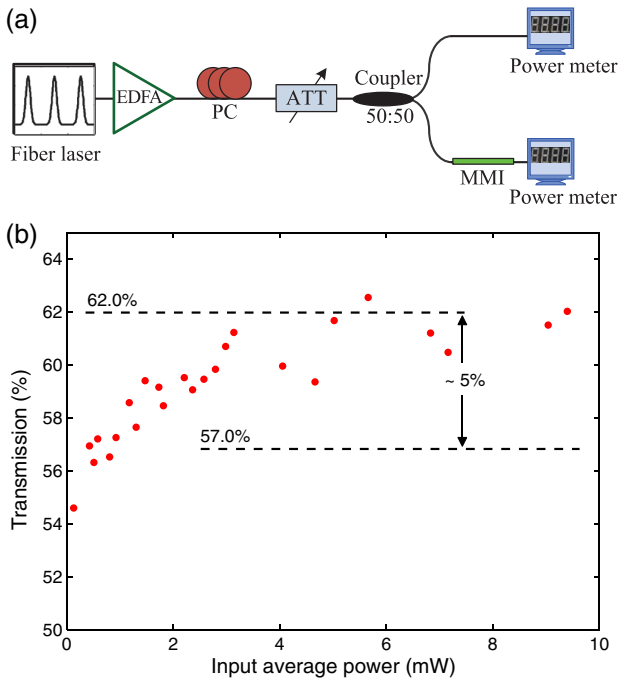

Fig. 4. (a) Experimental setup for the absorption measurement of the MMI structure. ATT, attenuator. (b) Measured nonlinear absorption of MMI structure with $L = 48.8$ mm.

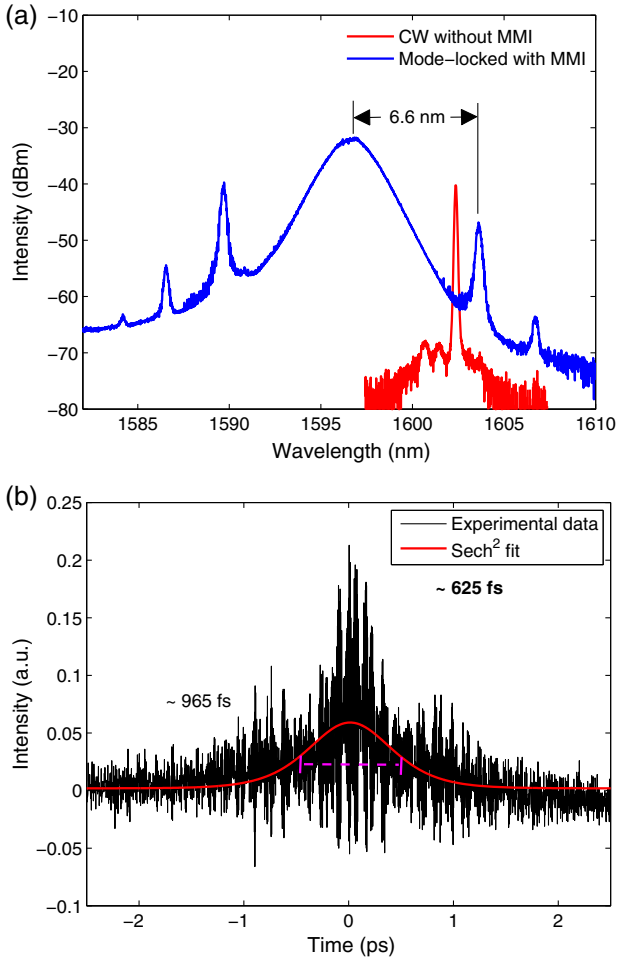

Fig. 5. (a) Output optical spectra of fiber laser for CW without MMI and mode-locked with MMI for underlying values. (b) Mode-locked pulse shape (experimental data) with sech^2 fit.

$$\Delta\lambda = \frac{2\ln(1+\sqrt{2})\lambda^2}{2\pi c\tau}\sqrt{\frac{4m\pi}{|L\beta_2|}\left[\frac{\tau}{2\ln(1+\sqrt{2})}\right]^2 - 1}, \tag{10}$$

where λ is the central wavelength, τ is the temporal width of the pulses, L is the cavity length, β_2 is the cavity dispersion, and the total cavity dispersion $|L\beta_2|$ is ~0.383 ps^2. The $\Delta\lambda$ for first-order Kelly sideband is 6.6 nm, as shown in Fig. 5(a), and the transform-limited τ is calculated to be ~587 fs by using Eq. (10). The actual pulse width is monitored by a second-harmonic-generation autocorrelator (APE pulseCheck). Figure 5(b) demonstrates the recorded autocorrelator trace of the laser pulses with a 5 ps scan range. Assuming a sech^2 profile, the trace width of ~965 fs can be obtained. Considering its decorrelation factor of 0.648, the actual pulse width is ~625 fs. The measured pulse width is larger than the theoretical value (τ = ~587 fs), indicating that the soliton pulses are small-chirped.

The pulse train of the laser output shown in Fig. 6(a) has a period of 114.6 ns, which matches well with the cavity's round-trip time and verifies that the laser is mode-locked. To study the operation stability, we have measured the radio frequency spectrum of the passively mode-locked fiber laser by the same high-speed photodetector (New Focus 1611, 1 GHz) connected to the mixed oscilloscope (Tektronix MDO 3102, Mixed Domain Oscilloscope). The fundamental peak is located at the repetition rate of 8.726 MHz, as shown in Fig. 6(b), with a signal-to-noise ratio of 65 dB. The inset of Fig. 6(b) shows the higher order of the harmonic radio frequency spectrum up to 200 MHz, and the achieved signal-to-noise ratio is degressive and also high, indicating good mode-locked stability. The average output power is ~1.75 mW, with the pulse energy of ~0.201 nJ.

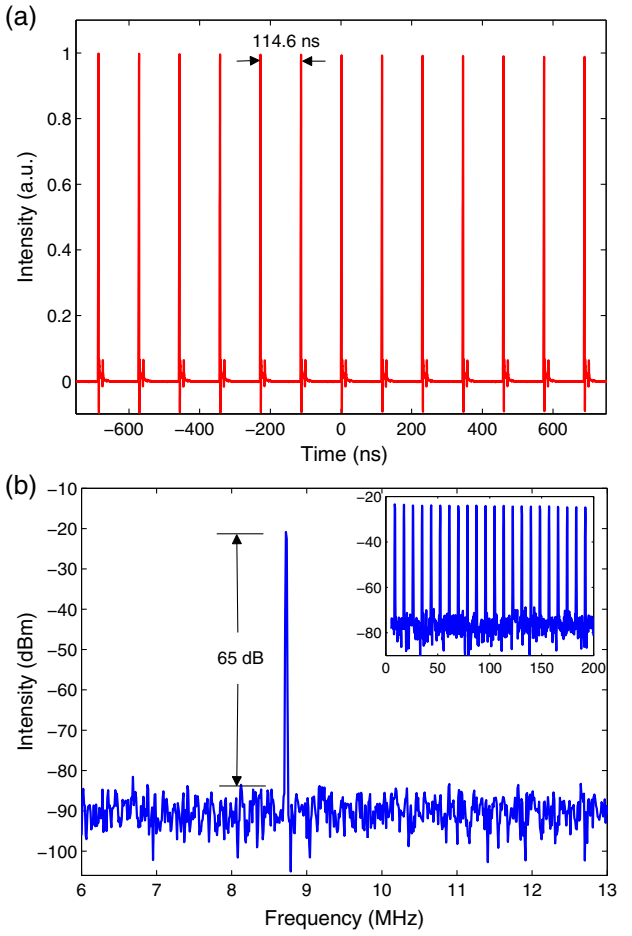

Fig. 6. (a) Typical laser output pulse train. (b) Radio frequency spectrum measured around the fundamental repetition rate. Inset is the radio frequency spectrum with high-order harmonic of the repetition rate.

Increasing the pump power to 101 mW, the pulse width suddenly increases to ~1.054 ps with almost invariable optical spectrum, and this phenomenon may arise from the nonlinearity of the fiber-induced chirp. The pump power can be increased to 227 mW, until the multipulse generation is observed. The maximal average output power can reach ~7.07 mW, with a pulse energy of ~0.810 nJ.

Total dispersion of the laser cavity is important for the formation of pulses. In the net anomalous dispersion regime, the soliton is formed due to the natural balance between the anomalous cavity dispersion and fiber third-order nonlinear optical effects, while in the net normal dispersion regime, the dissipative soliton is generated as a result of mutual nonlinear interaction among the normal cavity dispersion, fiber third-order nonlinearity, and the effective laser gain bandwidth filtering. With small net anomalous dispersion and net normal dispersion, the PC needs to be fine-tuned to start the mode-locking. In order to investigate the relationship between the pulses and the net cavity dispersion, the different lengths of SMF and DCF are added into the laser cavity, while other equipment remains unchanged. The GVD of the DCF is −30.5 ps/(nm·km) at the wavelength of 1560 nm. Figure 7 shows the optical spectra of output pulses with different lengths of SMF and DCF. For the net anomalous dispersion cases, the soliton optical spectra exhibit clear appearance of Kelly sidebands, while for the net normal dispersion case, the dissipative soliton optical spectrum exists, which is the characteristic of steep spectral edges, and the central wavelength is different from the solitons.

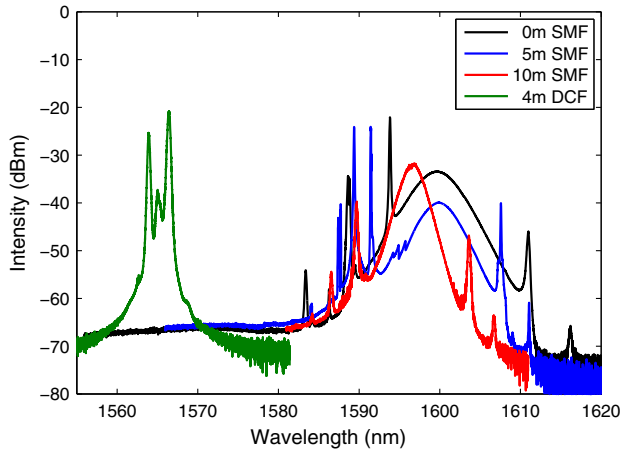

Fig. 7. Optical spectra of mode-locked fiber lasers for adding different lengths of SMF or DCF.

Table 1. Optical Parameters of Mode-Locked Fiber Laser for Adding Different Lengths of SMF and DCF

Added Fiber	Total Dispersion (ps^2)	Repetition Rate (MHz)	FWHM (nm)	Pulse Width (ps)	Pump Power Range (mW)	Output Power Range (mW)
0 m SMF	−0.139	16.05	4.64	0.973	92–140	1.6–3.07
5 m SMF	−0.261	10.98	4.24	0.958	52–70	0.67–1.09
10 m SMF	−0.383	8.726	2.18	0.625/1.054	56–97/101–227	0.84–1.78/1.85–7.07
4 m DCF	0.025	11.8	—	10,000	258–488	2.66–4.84

Table 1 summarizes the relationship between the total cavity dispersions and the laser characteristics. For the pump power range, the minimum is the mode-locking threshold when the maximum is the pulse-splitting threshold. While the total dispersions vary from −0.383 ps^2 to −0.139 ps^2, the increasing pulse widths hint that the pulses are with increasing chirps, and the FWHM of optical spectra increases from 2.18 to 4.64 nm at the repetition rates of 8.726–16.05 MHz. That is, the larger FWHMs are obtained with smaller net anomalous dispersion. In particular, the stable pulse width is 10 ns for 0.025-ps^2 total dispersion. The pump powers for this mode-locked state are from 258 to 488 mW, and the corresponding output powers are from 2.66 to 4.84 mW. Its mode-locking threshold is much larger than the ones for net anomalous dispersion cases. In addition, an unsteady mode-locked operation is also found in the experiment for net normal dispersion, the pulses may be the dissipative solitons, and the pulse width is to the subpicosecond. While all-normal dispersion fiber lasers have been studied extensively for exploiting dissipative soliton pulse dynamics, we will investigate the all-normal dispersion Yb-doped passively mode-locked fiber laser with nonlinear SIMF-based MMI in other work.

5. CONCLUSION

In conclusion, we have experimentally investigated the passively mode-locked fiber laser with nonlinear multimode interference of a step-index multimode fiber. The saturable absorption theory of nonlinear multimode interference with a multimode fiber is analyzed in detail. Using the nonlinear multimode interference structure with a 48.8 mm step-index multimode fiber, the all-fiber mode-locked fiber laser for different total cavity dispersion is studied systematically. The easy fabrication, good stability, and robust structure of the system will facilitate potential applications of nonlinear multimode interference structures with step-index multimode fiber in ultrafast photonics.

Funding. National Natural Science Foundation of China (NSFC) (11547187); Shandong Provincial Key RD Program (2017CXGC0416); Natural Science Foundation of Shandong Province (ZR2016FB17, ZR2017MA047).

REFERENCES

1. U. Keller, D. A. B. Miller, G. D. Boyd, T. H. Chiu, J. F. Ferguson, and M. T. Asom, "Solid-state low-loss intracavity saturable absorber for Nd:YLF lasers: an antiresonant semiconductor Fabry–Perot saturable absorber," Opt. Lett. **17**, 505–507 (1992).
2. S. Yamashita, Y. Inoue, S. Maruyama, Y. Murakami, H. Yaguchi, M. Jablonski, and S. Y. Set, "Saturable absorbers incorporating carbon nanotubes directly synthesized onto substrates and fibers and their application to mode-locked fiber lasers," Opt. Lett. **29**, 1581–1583 (2004).
3. A. Martinez, K. Zhou, I. Bennion, and S. Yamashita, "In-fiber microchannel device filled with a carbon nanotube dispersion for passive mode-lock lasing," Opt. Express **16**, 15425–15430 (2008).
4. F. Wang, A. Rozhin, V. Scardaci, Z. Sun, F. Hennrich, I. White, W. I. Milne, and A. C. Ferrari, "Wideband-tuneable, nanotube mode-locked, fibre laser," Nat. Nanotechnol. **3**, 738–742 (2008).
5. Q. Bao, H. Zhang, Y. Wang, Z. Ni, Y. Yan, Z. X. Shen, K. P. Loh, and D. Y. Tang, "Atomic-layer graphene as a saturable absorber for ultrafast pulsed lasers," Adv. Funct. Mater. **19**, 3077–3083 (2009).
6. Z. Sun, T. Hasan, F. Torrisi, D. Popa, G. Privitera, F. Wang, F. Bonaccorso, D. M. Basko, and A. C. Ferrari, "Graphene mode-locked ultrafast laser," ACS Nano **4**, 803–810 (2010).
7. X. He, Z. Liu, and D. N. Wang, "Wavelength-tunable, passively mode-locked fiber laser based on graphene and chirped fiber Bragg grating," Opt. Lett. **37**, 2394–2396 (2012).
8. T. Chen, C. Liao, D. Wang, and Y. Wang, "Passively mode-locked fiber laser by using monolayer chemical vapor deposition of graphene on D-shaped fiber," Appl. Opt. **53**, 2828–2832 (2014).
9. S. Wang, H. Yu, H. Zhang, A. Wang, M. Zhao, Y. Chen, L. Mei, and J. Wang, "Broadband few-layer MoS_2 saturable absorbers," Adv. Mater. **26**, 3538–3544 (2014).
10. H. Liu, A. Luo, F. Wang, R. Tang, M. Liu, Z. Luo, W. Xu, C. Zhao, and H. Zhang, "Femtosecond pulse erbium-doped fiber laser by a few-layer MoS_2 saturable absorber," Opt. Lett. **39**, 4591–4594 (2014).
11. P. Yan, A. Liu, Y. Chen, H. Chen, S. Ruan, C. Guo, S. Chen, I. L. Li, H. Yang, J. Hu, and G. Cao, "Microfiber-based WS_2-film saturable absorber for ultra-fast photonics," Opt. Mater. Express **5**, 479–489 (2015).
12. J. Sotor, G. Sobon, K. Grodecki, and K. M. Abramski, "Mode-locked erbium-doped fiber laser based on evanescent field interaction with Sb_2Te_3 topological insulator," Appl. Phys. Lett. **104**, 251112 (2014).
13. Y. H. Lin, S. F. Lin, Y. C. Chi, C. L. Wu, C. H. Cheng, W. H. Tseng, J. H. He, C. I. Wu, C. K. Lee, and G. R. Lin, "Using n- and p-type Bi_2Te_3 topological insulator nanoparticles to enable controlled femtosecond mode-locking of fiber lasers," ACS Photon. **2**, 481–490 (2015).
14. Y. Song, S. Chen, Q. Zhang, L. Li, L. Zhao, H. Zhang, and D. Tang, "Vector soliton fiber laser passively mode locked by few layer black phosphorus-based optical saturable absorber," Opt. Express **24**, 25933–25942 (2016).
15. S. Liu, Z. Li, Y. Ge, H. Wang, R. Yue, X. Jiang, J. Li, Q. Wen, and H. Zhang, "Graphene/phosphorene nano-heterojunction: facile synthesis, nonlinear optics, and ultrafast photonics applications with enhanced performance," Photon. Res. **5**, 662–668 (2017).
16. S. Y. Ryu, K. S. Kim, J. Kim, and S. Kim, "Degradation of optical properties of a film-type single-wall carbon nanotubes saturable absorber (SWNT-SA) with an Er-doped all-fiber laser," Opt. Express **20**, 12966–12974 (2012).
17. A. Martinez, K. Fuse, and S. Yamashita, "Enhanced stability of nitrogen-sealed carbon nanotube saturable absorbers under high-intensity irradiation," Opt. Express **21**, 4665–4670 (2013).
18. V. J. Matsas, T. P. Newson, D. J. Richardson, and D. N. Payne, "Self-starting passively mode-locked fiber ring soliton laser exploiting nonlinear polarization rotation," Electron. Lett. **28**, 1391–1393 (1992).
19. Z. Yan, X. Li, Y. Tang, P. P. Shum, X. Yu, Y. Zhang, and Q. J. Wang, "Tunable and switchable dual-wavelength Tm-doped mode-locked fiber laser by nonlinear polarization evolution," Opt. Express **23**, 4369–4376 (2015).

20. M. E. Fermann, F. Haberl, M. Hofer, and H. Hochreiter, "Nonlinear amplifying loop mirror," Opt. Lett. **15**, 752–754 (1990).
21. C. Aguergaray, N. G. R. Broderick, M. Erkintalo, J. S. Y. Chen, and V. Kruglov, "Mode-locked femtosecond all-normal all-PM Yb-doped fiber laser using a nonlinear amplifying loop mirror," Opt. Express **20**, 10545–10551 (2012).
22. J. Proctor and J. N. Kutz, "Nonlinear mode-coupling for passive mode-locking: application of waveguide arrays, dual-core fibers, and/or fiber arrays," Opt. Express **13**, 8933–8950 (2005).
23. Q. Chao, D. D. Hudson, J. N. Kutz, and S. T. Cundiff, "Waveguide array fiber laser," IEEE Photon. J. **4**, 1438–1442 (2012).
24. E. Nazemosadat and A. Mafi, "Saturable absorption in multicore fiber couplers," J. Opt. Soc. Am. B **30**, 2787–2790 (2013).
25. H. G. Winful and D. T. Walton, "Passive mode locking through nonlinear coupling in a dual-core fiber laser," Opt. Lett. **17**, 1688–1690 (1992).
26. Y. Oh, S. L. Doty, J. W. Haus, and R. L. Fork, "Robust operation of a dual-core fiber ring laser," J. Opt. Soc. Am. B **12**, 2502–2507 (1995).
27. T. F. S. Büttner, D. D. Hudson, E. C. Mägi, A. C. Bedoya, T. Taunay, and B. J. Eggleton, "Multicore, tapered optical fiber for nonlinear pulse reshaping and saturable absorption," Opt. Lett. **37**, 2469–2471 (2012).
28. A. S. Karar, T. Smy, and A. L. Steele, "Nonlinear dynamics of a passively mode-locked fiber laser containing a long-period fiber grating," IEEE J. Quantum Electron. **44**, 254–261 (2008).
29. E. Nazemosadat and A. Mafi, "Nonlinear multimodal interference and saturable absorption using a short graded-index multimode optical fiber," J. Opt. Soc. Am. B **30**, 1357–1367 (2013).
30. W. S. Mohammed, P. W. E. Smith, and X. Gu, "All-fiber multimode interference bandpass filter," Opt. Lett. **31**, 2547–2549 (2006).
31. A. Castillo-Guzman, J. E. Antonio-Lopez, R. Selvas-Aguilar, D. A. May-Arrioja, J. Estudillo-Ayala, and P. LiKamWa, "Widely tunable erbium-doped fiber laser based on multimode interference effect," Opt. Express **18**, 591–597 (2010).
32. X. Zhu, A. Schülzgen, H. Li, L. Li, Q. Wang, S. Suzuki, V. L. Temyanko, J. V. Moloney, and N. Peyghambarian, "Single-transverse-mode output from a fiber laser based on multimode interference," Opt. Lett. **33**, 908–910 (2008).
33. X. Zhu, A. Schülzgen, H. Li, H. Wei, J. V. Moloney, and N. Peyghambarian, "Coherent beam transformations using multimode waveguides," Opt. Express **18**, 7506–7520 (2010).
34. A. B. Socorro, I. D. Villar, J. M. Corres, F. J. Arregui, and I. R. Matias, "Mode transition in complex refractive index coated single-mode-multimode–single-mode structure," Opt. Express **21**, 12668–12682 (2013).
35. N. Bhatia and J. John, "Multimode interference devices with single-mode-multimode–multimode fiber structure," Appl. Opt. **53**, 5179–5186 (2014).
36. N. Bhatia, K. C. Rustagi, and J. John, "Single $LP_{0,n}$ mode excitation in multimode fibers," Opt. Express **22**, 16847–16862 (2014).
37. N. Bhatia and J. John, "Single-mode-multimode-multimode device: sensitivity of the single mode to the fiber parameters and geometrical misalignments," J. Opt. Soc. Am. B **33**, 211–219 (2016).
38. L. G. Wright, Z. Liu, D. A. Nolan, M. J. Li, D. N. Christodoulides, and F. W. Wise, "Self-organized instability in graded-index multimode fibres," Nat. Photonics **10**, 771–776 (2016).
39. L. G. Wright, D. N. Christodoulides, and F. W. Wise, "Spatiotemporal mode-locking in multimode fiber lasers," Science **358**, 94–97 (2017).
40. A. Mafi, P. Hofmann, C. J. Salvin, and A. Schülzgen, "Low-loss coupling between two single-mode optical fibers with different mode-field diameters using a graded-index multimode optical fiber," Opt. Lett. **36**, 3596–3598 (2011).
41. P. Hofmann, A. Mafi, C. Jollivet, T. Tiess, N. Peyghambarian, and A. Schulzgen, "Detailed investigation of mode-field adapters utilizing multimode-interference in graded index fibers," J. Lightwave Technol. **30**, 2289–2298 (2012).
42. H. Li, Z. Wang, C. Li, J. Zhang, and S. Xu, "Mode-locked Tm fiber laser using SMF-SIMF-GIMF-SMF fiber structure as a saturable absorber," Opt. Express **25**, 26546–26553 (2017).
43. Z. Wang, D. Wang, F. Yang, L. Li, C. Zhao, B. Xu, S. Jin, S. Cao, and Z. Fang, "Er-doped mode-locked fiber laser with a hybrid structure of step index-graded index multimode fiber as the saturable absorber," J. Lightwave Technol. **35**, 5280–5285 (2017).
44. F. Yang, D. N. Wang, Z. Wang, L. Li, C. Zhao, B. Xu, S. Jin, S. Cao, and Z. Fang, "Saturable absorber based on a single mode fiber-graded index fiber-single mode fiber structure with inner micro-cavity," Opt. Express **26**, 927–934 (2018).
45. Z. Wang, D. N. Wang, F. Yang, L. Li, C. Zhao, B. Xu, S. Jin, S. Cao, and Z. Fang, "Stretched graded-index multimode optical fiber as a saturable absorber for erbium-doped fiber laser mode locking," Opt. Lett. **43**, 2078–2081 (2018).
46. U. Teğin and B. Ortaç, "All-fiber all-normal-dispersion femtosecond laser with a nonlinear multimodal interference-based saturable absorber," Opt. Lett. **43**, 1611–1614 (2018).
47. X. Zhu, *Multimode Interference in Optical Fibers and its Applications of Fiber Lasers and Amplifiers* (University of Arizona, 2008).
48. Q. Wang, G. Farrell, and W. Yan, "Investigation on single-mode-multimode–single-mode fiber structure," J. Lightwave Technol. **26**, 512–519 (2008).
49. S. Fu, Q. Sheng, X. Zhu, W. Shi, J. Yao, G. Shi, R. A. Norwood, and N. Peyghambarian, "Passive *Q*-switching of an all-fiber laser induced by the Kerr effect of multimode interference," Opt. Express **23**, 17255–17262 (2015).
50. H. Li, M. Brio, L. Li, A. Schülzgen, N. Peyghambarian, and J. V. Moloney, "Multimode interference in circular step-index fibers studied with the mode expansion approach," J. Opt. Soc. Am. B **24**, 2707–2720 (2007).
51. T. Chen, J. Sun, and L. Li, "Modal theory of slow light enhanced third-order nonlinear effects in photonic crystal waveguides," Opt. Express **20**, 20043–20058 (2012).
52. G. P. Agrawal, *Nonlinear Fiber Optics and Applications of Nonlinear Fiber Optics*, 4th ed. (Elsevier, 2007).
53. H. Afkhamiardakani, M. Tehrani, and J.-C. Diels, "Extension of the stable operation of an all polarization maintaining mode-locked fiber laser," in *Conference on Lasers and Electro-Optics* (Optical Society of America, 2018), paper JTh2A.141.
54. N. J. Smith, K. J. Blow, and I. Andonovic, "Sideband generation through perturbations to the average soliton model," J. Lightwave Technol. **10**, 1329–1333 (1992).
55. M. Jung, J. Koo, J. Park, Y.-W. Song, Y. M. Jhon, K. Lee, S. Lee, and J. H. Lee, "Mode-locked pulse generation from an all-fiberized, Tm-Ho-codoped fiber laser incorporating a graphene oxide-deposited side-polished fiber," Opt. Express **21**, 20062–20072 (2013).